water

MDPI

*Article*

# Comparative Assessment of D8 and D∞ Algorithms for Drainage Delineation and Digital Terrain Model Resolution Effects on Environmental Sensitivity Mapping

**Paulo Henrique Lopes da Rosa [1,*], Daiana Petry Rufato [1], Eder Alexandre Schatz Sá [2], Leonardo Josoé Biffi [1] and Natan Andrade Neto da Silva [1]**

[1] Department of Environmental and Sanitary Engineering, Santa Catarina State University, Lages 88520-000, Brazil; daiana.petry@udesc.br (D.P.R.); natan.silva@edu.udesc.br (N.A.N.d.S.)
[2] Department of Forest Engineering, Unicentro University, Irati 84500-000, Brazil
* Correspondence: paulo.rosa8@edu.udesc.br

**Abstract**

Drainage products derived from digital terrain models (DTMs) depend on resolution, flow routing, and channel-initiation thresholds. This study compared the Deterministic Eight (D8) and D-infinity (D∞) algorithms for drainage delineation in the 26.9 km$^2$ Ponte Grande River watershed, Lages, Brazil. Height Above the Nearest Drainage (HAND) and Topographic Wetness Index (TWI) maps were derived from D8 only. A 1 m DTM (2012 aerial survey) was aggregated to 5, 10, and 30 m and conditioned in TauDEM. Thresholds were tuned visually for each configuration against the Santa Catarina state hydrography (SIGSC); no positional-accuracy metrics or flood records were used. The 1 and 5 m DTMs produced dense, microtopography-driven networks (up to 1.99 km/km$^2$) and fragmented HAND and TWI patterns. D∞ produced more diffuse flow, whereas D8 produced more concentrated, hierarchical networks, a criterion that favors D8 by construction. The 10 and 30 m DTMs gave the more interpretable outputs; D8 at 30 m had the lowest drainage density (0.76 km/km$^2$), partly because of its larger threshold. Thresholds differed among configurations and were tuned against the same reference, so algorithm, resolution, and threshold effects are confounded and agreement may favor coarser DTMs. HAND and TWI are topographic proxies; linking them to flooding requires hydraulic or event data.

**Keywords:** flow direction; drainage networks; digital terrain model; HAND; topographic wetness index; urban watershed; environmental sensitivity mapping

Check for updates

Academic Editor: Salvatore Ivo Giano

Received: 1 October 2026
Revised: 23 October 2026
Accepted: 28 October 2026
Published: 9 November 2026

**Copyright:** © 2026 by the authors. Licensee MDPI, Basel, Switzerland. This article is an open access article distributed under the terms and conditions of the Creative Commons Attribution (CC BY) license.

## 1. Introduction

Urban flooding and the degradation of environmentally sensitive areas have become increasingly frequent in Brazilian watersheds [1,2]. This trend is especially evident under unplanned urban expansion and increasing soil imperviousness [1,2]. These dynamics alter watershed hydrological behavior by increasing surface runoff, which may exceed drainage system capacity.

The accurate delineation of the drainage network and the identification of areas susceptible to saturation and flooding are fundamental for urban and environmental planning. Digital Terrain Models (DTMs) have been widely combined with hydromorphological indices for the rapid, low-cost screening of vulnerable areas [3–5]. These indices include the Height Above the Nearest Drainage (HAND) and the Topo graphic Wetness Index (TWI).

However, the outputs of these models depend, among other factors, on the flow-direction algorithm, which defines how surface runoff is distributed across the terrain.

Two of the most widely used flow-direction algorithms are Deterministic Eight (D8) and D-infinity (D∞). D8 assigns flow to the neighboring cell with the steepest slope. D∞ represents flow direction as a continuous angle and partitions flow between the two adjacent downslope cells according to the topographic gradient [6]. Tarboton [6] showed that D∞ represents divergent hillslope flow better than single-direction methods. In contrast, D8 concentrates flow into discrete, single-cell paths.

Several studies have examined how DTM-derived drainage products respond to the flow-direction algorithm, DTM resolution, and channel-initiation threshold. Tarboton [6] proposed the D∞ algorithm. Quinn et al. [7] introduced a multiple-flow-direction (MFD) approach for hillslope flow paths. Wolock and McCabe [8] showed that single- and multiple-flow-direction algorithms yield different TWI distributions. Silveira and Silveira [9] applied D∞ contributing area to map hilltops, ridges, and valleys. These studies indicate that the choice of algorithm can substantially alter the structure of the simulated drainage network and the spatial patterns of flow accumulation. In the Brazilian context, Guasselli et al. [4] discuss the sensitivity of these models to DTM resolution and to the adopted accumulation thresholds. Together, these studies show that the flow algorithm, the DTM resolution, and the drainage-extraction threshold jointly influence the hydrological representation of the watershed.

Because these factors interact, visual comparison alone cannot separate the effect of the algorithm from those of resolution and threshold. Comparisons of D8 and D∞ therefore require quantifiable evaluation criteria. Examples include positional agreement with reference hydrography, drainage density, and the response of network length to the threshold. Such criteria should be applied under common, equivalent thresholds. Single-direction routing tends to concentrate TWI into narrow, striped paths on divergent hillslopes [6,7]. Dispersion of flow on hillslopes, which affects TWI, is what D∞ and MFD routing were proposed to represent [6,7]. It is also established that TWI and its components change markedly with DTM resolution [10].

In this context, this study compares the D8 and D∞ algorithms in the Ponte Grande River watershed, Lages, Santa Catarina, Brazil. The algorithm comparison covers drainage network extraction only. HAND and TWI maps were derived from D8 to describe resolution effects under a single routing scheme. The study applies explicit evaluation criteria: geomorphological coherence, stability across channel-initiation thresholds, visual agreement with the SIGSC hydrographic reference, and the visual interpretability of the D8-based HAND and TWI maps. Drainage length and density (Table 1) support these criteria and are reported quantitatively, whereas positional agreement was assessed only visually. The study thus documents which criteria still require quantitative metrics. The choice of algorithm can influence network morphology, contributing-area distribution, and the spatial pattern of topographic wetness proxies [6,8]. Terrain-based mapping of this kind is often proposed to support urban flood-risk planning [3,5]. Here, the contribution is an application restricted to the Ponte Grande River watershed, without claims of methodological novelty. Resolution-dependent TWI patterns in fine DTMs are thus an expected result [10]. The study documents the processing steps and parameter ranges applied in this watershed, without independent validation of the resulting products.

**Table 1.** Drainage extraction sensitivity analysis across DTM resolutions and flow direction algorithms.

| Algorithm (DTM) | Threshold Range (Native Units) | Equivalent Contributing Area ($km^2$) | Mean Total Length (km) | Drainage Density ($km/km^2$) |
|---|---|---|---|---|
| D8 (30 m) | 100–1000 | 0.09–0.90 | 20.40 | 0.76 |
| D8 (10 m) | 1500–2500 | 0.15–0.25 | 34.82 | 1.29 |
| D8 (5 m) | 3000–9000 | 0.08–0.23 | 37.11 | 1.38 |
| D8 (1 m) | 90,000–110,000 | 0.09–0.11 | 53.41 | 1.99 |
| D∞ (30 m) | 3000–9000 | 0.09–0.27 | 32.16 | 1.20 |
| D∞ (10 m) | 10,000–30,000 | 0.10–0.30 | 33.04 | 1.23 |
| D∞ (5 m) | 40,000–80,000 | 0.20–0.40 | 36.73 | 1.37 |
| D∞ (1 m) | 120,000–200,000 | 0.12–0.20 | 40.69 | 1.51 |

## 2. Materials and Methods

This section describes the materials, data, and procedures adopted. These include the study area characterization, topographic and thematic processing, and the stages of spatial modeling. It details the generation of Digital Terrain Models (DTMs), the application of the D8 and D∞ algorithms, and the derivation of the HAND and TWI indices. It also describes the threshold selection criteria and the sensitivity analysis. Networks were compared visually with the hydrographic reference of the Geographic Information System of Santa Catarina (SIGSC).

### *2.1. Study Area*

The study area comprises the Ponte Grande River watershed (26.9 $km^2$), part of the Caveiras River system (Figure 1). This watershed encompasses a large portion of the urban area of the municipality of Lages (SC), a region historically affected by recurrent urban flooding events [5].

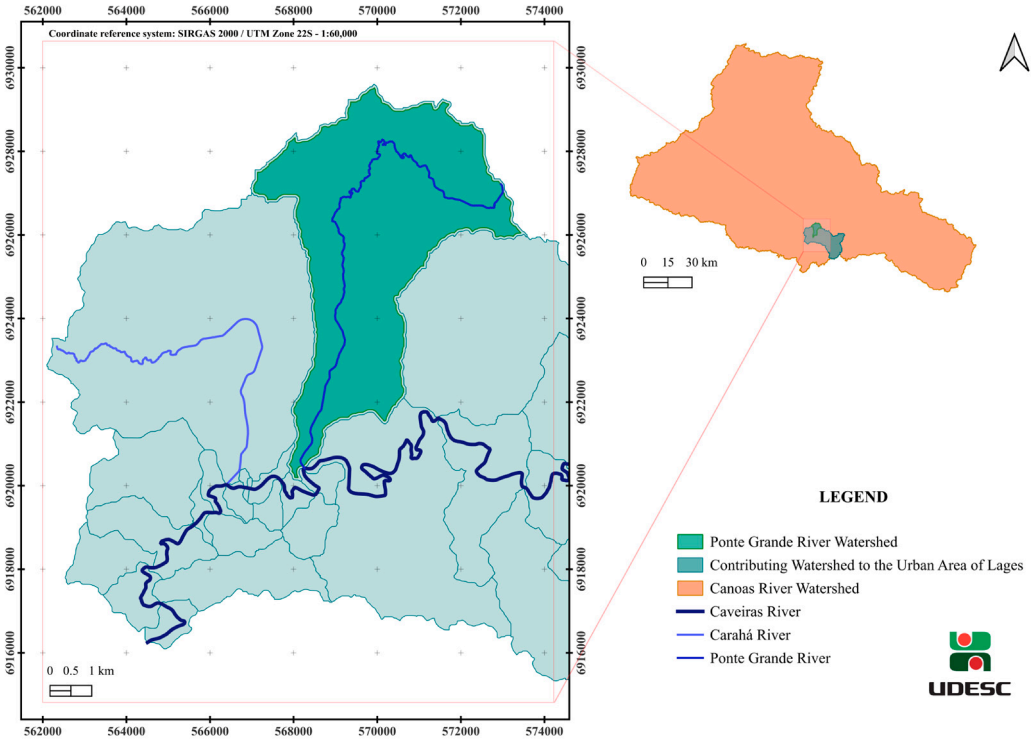


**Figure 1.** Location and Hydrography of the Ponte Grande River Watershed.

The spatial characterization of the drainage network was based on the hydrographic database provided by SIGSC. The Caveiras River watershed, within which the Ponte Grande River watershed is located, lies in the Santa Catarina Plateau and is part of the Water Resources Planning Unit RH4–Planalto de Lages, belonging to the Uruguay Hydrographic Region. These units have distinct physiographic configurations, multiple water uses, and hydrological regimes, which are fundamental for regional water resources planning and management [11]. Historically, the Caveiras watershed experienced significant flood events in 2005, 2008, and 2011, particularly in urban areas, demonstrating its vulnerability to intense precipitation events and rapid hydrological response [11]. These events are reported here as regional context only; no records of flood extent or flood occurrence were used in the analyses of this study.

The Ponte Grande River watershed has mixed land use. Its urbanized portion concentrates high urban occupation and industrial activities, while the upstream portion is predominantly rural, composed of pasturelands, reforestation areas, and remnants of Atlantic Forest with Araucaria. Approximately one-third of the watershed is urbanized, while the remaining two-thirds correspond to rural areas [12].

The watershed is entirely located within the Atlantic Forest biome, with potential vegetation characterized by Mixed Ombrophilous Forest, including Araucaria angustifolia and broadleaf species such as imbuia and cedar. In Lages, current vegetation forms a mosaic of high-altitude grasslands, reforestation areas, and secondary Araucaria forests, with local initiatives focused on forest recovery and conservation [13]. Land use and land cover data were obtained from MapBiomas Collection 8 [12], which provides annual land cover mapping at 30 m resolution based on Landsat image time series and machine learning algorithms. These data were used only as contextual information on the distribution of impervious urban areas, remaining vegetation, and other classes such as agriculture and water bodies. Land use and land cover were not used as inputs to the HAND or TWI computations, and their influence on runoff generation and soil saturation was not quantified in this study.

The climate of Lages is characteristic of the Santa Catarina Plateau, marked by high altitudes, a strong influence of frontal systems, and significant meteorological variability throughout the year. According to the Köppen–Geiger classification, the region is predominantly classified as humid subtropical (Cfb), with no defined dry season, mild summers, and cold winters, often with frost [14]. Rainfall is relatively well distributed throughout the year, with annual precipitation ranging from 1200 to 2300 mm. The average annual temperature varies between 15 °C and 18 °C, with slightly lower values due to higher altitude and greater exposure to polar air masses during winter [15,16].

The Ponte Grande River watershed is predominantly composed of clayey Haplic Cambisols and localized areas of shallow soils on steep slopes. Cambisols, characterized by fine texture and moderate depth, are generally associated with low infiltration rates (approximately 1 mm/h, an indicative value from the literature rather than a measurement in the study watershed), which can favor Hortonian surface runoff, especially during high-intensity rainfall events [17,18]. Low infiltration may also limit percolation to deeper layers, resulting in localized surface saturation without full soil profile saturation [19].

Shallow or transitional soils, often associated with rocky substrates or impermeable layers and steep terrain, have very limited water storage capacity. These conditions can lead to rapid saturation even under moderate rainfall. Saturation-excess overland flow occurs where the soil becomes saturated up to the surface [20]. The combination of shallow depth and steep slopes can result in a rapid hydrological response to rainfall and high peak flows [18,21].

Overall, this physical setting suggests that the watershed is sensitive to intense rainfall, with surface runoff potentially generated by different mechanisms: infiltration excess in Cambisols and saturation excess in shallow soils. This characterization is contextual; it was not quantified or validated in the present study, and its relationship with the results is discussed interpretatively in Section 3.4.

### *2.2. Hydromorphological Model Configuration*

The methodology was structured in a sequential and comparative manner. It evaluated the influence of Digital Terrain Model (DTM) resolution, flow-direction algorithm (D8 and D∞), and channel-initiation threshold on drainage extraction. It also evaluated the influence of resolution on D8-based HAND and TWI maps, used as topographic proxies. The procedure included raw DTM processing and hydrological conditioning in TauDEM (Terrain Analysis Using Digital Elevation Models). It then comprised flow-direction modeling, contributing-area calculation, and threshold-based drainage network definition. HAND and TWI maps were then generated from these inputs and compared, as summarized in the methodological flowchart in Figure 2.

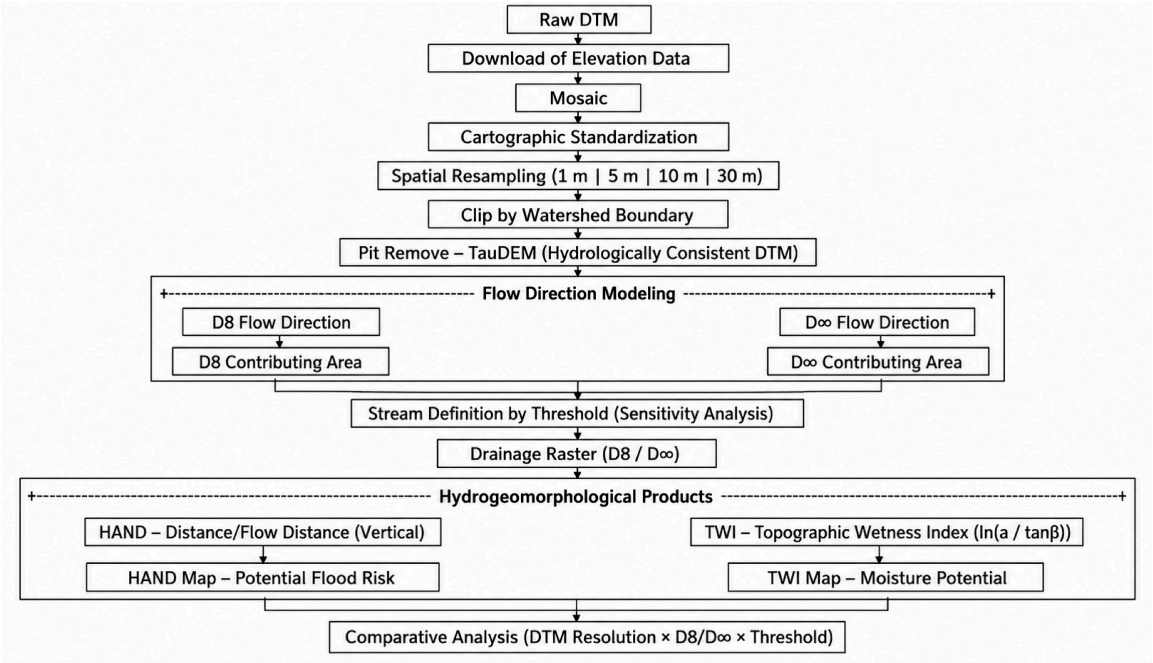


**Figure 2.** Methodological flowchart. Arrows indicate the processing sequence; dashed lines ending in "+" markers head the framed blocks that group steps performed in parallel (D8 and D∞ flow-direction modeling; HAND and TWI products).

#### 2.2.1. Digital Terrain Model

The 1 m Digital Terrain Model (DTM) was obtained from SIGSC and derives from an aerial survey conducted in 2012. According to the official SIGSC raster metadata, the statewide survey was conducted between 2010 and 2012 [22]. The metadata report a spatial resolution of 1.00 m and an altimetric precision of 1.00 m for the DTM [22]. They do not state whether this value is an RMSE or a cartographic accuracy class. The 5, 10, and 30 m DTMs are not independent products. They were obtained by mean aggregation of the original 1 m DTM. Mean aggregation was adopted because averaging the 1 m cells within each coarser cell acts as a low-pass filter. This attenuates short-wavelength altimetric noise and microrelief. The aggregated DTMs therefore differ from DTMs natively produced at 5, 10, or 30 m. Native products have their own acquisition, interpolation, and error

characteristics. All DTM versions then underwent hydrological correction in ArcGIS 10.5 (Esri, Redlands, CA, USA) with the TauDEM extension (Utah State University, Logan, UT, USA). This correction included the filling of spurious depressions and the smoothing of altimetric noise. Because the DTM represents terrain conditions in 2012, anthropogenic features built or modified after the survey (e.g., cuts, fills, and roads) are not represented in the terrain surface. As the MapBiomas land use and land cover data refer to a different period, interpretations involving anthropogenic features are qualitative.

#### 2.2.2. Terrain Preparation and Hydrological Conditioning

Initially, the DTM was subjected to hydrological conditioning, with the removal of artificial depressions (sinks) that could improperly interrupt natural surface runoff paths. This step was performed using the Pit Remove algorithm, available in the TauDEM package, ensuring topographic connectivity and hydrological consistency of the terrain. This procedure is essential to guarantee that all cells in the model have hydraulic continuity toward the watershed outlet.

#### 2.2.3. Flow Direction Modeling

After hydrological conditioning of the DTM, surface flow direction was determined using two distinct algorithms: D8 (Deterministic Eight) and D∞ (D-infinity), both implemented in the TauDEM environment, with the objective of evaluating the sensitivity of drainage extraction to the flow routing method.

The D8 algorithm assigns each cell a single flow direction, corresponding to the steepest downward slope relative to its eight neighboring cells, representing concentrated and well-defined flows. In contrast, the D∞ algorithm, proposed by Tarboton [6], defines flow direction as a continuous angle, allowing flow distribution between two adjacent cells, which is generally considered to represent divergent flow in convex areas and smooth surfaces more realistically [6]. The difference between the algorithms is illustrated in Figure 3.

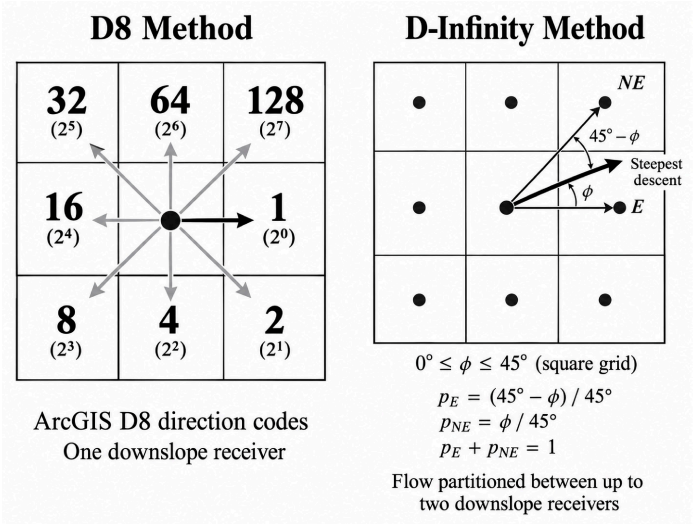


**Figure 3.** Comparison between D8 and D∞ algorithms. Source: O'Callaghan and Mark [23] and Tarboton [6]. Adapted using Gemini Pro (2026).

The combined application of both algorithms allowed comparison of the drainage networks obtained with each routing method.

#### 2.2.4. Contributing Area Calculation

Based on the D8 and D∞ flow-direction rasters, the accumulated contributing area was calculated using the D8 Contributing Area and D-Infinity Contributing Area tools, respectively. This operation determines, for each cell, the upslope area draining through it (expressed as the number of contributing cells for D8 and as specific catchment area for D∞), functioning as an indicator of surface flow convergence across the terrain. According to the TauDEM documentation, the D∞ output is the flow-weighted count of contributing cells multiplied by the cell size. It is thus expressed in meters, as contributing area per unit contour width equal to the cell size.

The flow accumulation raster represents a fundamental input for both drainage network delineation and the application of topographic indices, as it expresses the spatial organization of hydrological contribution throughout the landscape.

#### 2.2.5. Drainage Network Extraction

The drainage network was extracted from the contributing area raster by applying a minimum contributing-area threshold. Cells whose accumulated area exceeded this value were classified as part of the drainage network, generating a synthetic drainage network consistent with the watershed's topographic structure.

Thresholds were selected separately for each combination of flow-direction algorithm and DTM resolution. Thresholds were varied within the ranges reported in Table 1, in the native units of each contributing-area raster. Within each range (100 to 200,000), values were tested at increments of 200, 500, 1000, 5000, and 10,000 native units (cells for D8; meters of specific catchment area for D∞).

The SIGSC hydrography was the primary reference for evaluating the resulting networks. High-resolution Google Satellite imagery (Google LLC, Mountain View, CA, USA) was used only as a secondary visual aid. A threshold was retained when the network met two criteria relative to the SIGSC hydrography. First, the main tributaries mapped in SIGSC were represented. Second, no artificial over-densification by spurious first-order segments was observed. For each configuration, the ranges in Table 1 contain the thresholds that best met these two criteria; for the 1 and 5 m DTMs, no tested threshold satisfied both simultaneously (Sections 3.2 and 3.4). These criteria were applied by visual inspection, without an automated decision rule. Thresholds were therefore tuned visually against the same SIGSC hydrography later used to judge agreement. Each configuration was tuned separately. The study thus compares separately tuned configurations, not algorithms or resolutions in isolation.

The total length and drainage density in Table 1 are mean values across the thresholds tested within these ranges. The equivalent contributing area in Table 1 is the threshold multiplied by the cell area for D8 ($N \cdot \Delta x^2$) and by the cell size for D∞ (specific catchment area $\times \Delta x$). Objective alternatives were not applied, such as a length–threshold curve plateau or buffer-based agreement with SIGSC. Threshold stability was assessed qualitatively as the degree to which the network configuration changed across the tested range. This step is particularly relevant for the HAND model application, as the spatial configuration of the drainage network directly influences vertical distance calculations.

#### 2.2.6. HAND Model

Height Above the Nearest Drainage (HAND) was calculated for each spatial resolution from the hydrologically conditioned DTM and the drainage network extracted at that resolution. All HAND calculations were performed with TauDEM as an extension of ArcGIS 10.5. For D8, HAND was calculated as the elevation difference between each cell and the first drainage cell reached along its single downstream flow path. The inputs

comprised the conditioned elevation raster, the D8 flow-direction raster, and a binary drainage raster (stream cells = 1; other cells = 0). All rasters used the SIRGAS 2000/UTM zone 22S coordinate reference system, with coordinates and elevations in meters. Within each resolution scenario, all rasters shared the same grid alignment and extent. The resulting HAND maps were compared across the 1, 5, 10, and 30 m DTMs. Five environmental sensitivity classes were mapped: very high, high, moderate, low, and very low. They were interpreted as floodplain, transitional, middle-slope, upper-slope, and interfluve environments, respectively. HAND is a terrain descriptor of vertical proximity to the nearest channel, not a model of flood depth or hazard. Linking HAND classes to flooding would require hydraulic or event data, which were not used here.

The HAND value corresponds to the vertical elevation difference between the analyzed cell and the corresponding drainage point, expressing the relative height above the nearest channel. Only the D8-based HAND is presented and analyzed (Section 3.3). Therefore, the influence of the flow-direction method on HAND was not evaluated.

The five classes follow the conceptual framework of Rennó et al. [24] and Nobre et al. [25], who related HAND values to hydrologically distinct landscape units. The class limits were then adjusted iteratively by testing different HAND thresholds and inspecting the resulting spatial differentiation of morpho-hydrological compartments.

#### 2.2.7. Topographic Wetness Index

The Topographic Wetness Index (TWI) was calculated using Equation (1), following the classical formulation proposed by Beven and Kirkby [26]:

$$\mathrm{TWI} = \ln\left(\frac{a}{\tan\beta}\right) \tag{1}$$

where $a$ is the specific contributing area, i.e., the upslope contributing area per unit contour width (m), derived from the D8 contributing-area raster. In Equation (1), $\beta$ is the local slope angle obtained from the DTM. The accumulated number of contributing cells ($N$) was multiplied by the cell area and divided by the contour width. The contour width was taken as the cell size $\Delta x$, so that $a = N \cdot \Delta x$. The TWI maps presented in Section 3.3 were derived from the D8 configuration.

TWI expresses the relative topographic potential of each cell for water accumulation, integrating information on flow convergence and local topographic control. High TWI values are associated with flat and convergent areas, while low values indicate better-drained topographic positions.

### *2.3. AI Tools Disclosure*

Generative artificial intelligence tools were used exclusively for limited editorial and illustrative purposes. AI assistance (Claude; Anthropic, San Francisco, CA, USA) was employed to improve the English translation and linguistic clarity of the manuscript, without altering its scientific content, interpretation, methodology, or conclusions. In addition, Gemini Pro (Google LLC, Mountain View, CA, USA) was used to assist in the graphical refinement of Figure 3, a conceptual illustration comparing the D8 and D∞ flow-direction schemes; however, the scientific concepts represented in this figure were based exclusively on the original sources cited in the figure caption and in the manuscript. No artificial intelligence tools were used for data generation or processing, hydrological analysis, model execution, statistical analysis, interpretation of results, or scientific decision-making. All AI-assisted content was reviewed and validated by the authors, who take full responsibility for the final content of the manuscript.

## 3. Results and Discussion

The scenarios were evaluated using four criteria. The first three were the geomorphological coherence of the extracted network, its stability across channel-initiation thresholds, and its visual agreement with the SIGSC reference. Satellite imagery was used only to support the visual presence of channels. It does not validate flood or saturation zones. The fourth criterion was the visual cartographic interpretability of the derived HAND and TWI products. The comparison was based on visual cartographic inspection, supported by the drainage length and density values in Table 1. No quantitative agreement metric was computed. All statements on agreement in Section 3 therefore refer to visual cartographic adequacy. Comparing the 1, 5, 10, and 30 m products shows how topographic detail influences the drainage network and the derived topographic indices. The relationship among DTM resolution, threshold definition, and the scale of the hydrological process analyzed is a relevant factor for interpreting the results. This is consistent with studies reporting that topographic-index-based mapping is highly sensitive to DTM quality, resolution, and drainage network definition [5,24,25,27].

### *3.1. Comparison of D8 and D∞*

To compare the drainage networks derived using D8 and D∞, a qualitative visual assessment was conducted against the SIGSC hydrographic reference. The algorithms were compared separately at each DTM resolution (1, 5, 10, and 30 m). The comparison considered apparent centerline alignment, lateral deviations, tributary representation, and additional or omitted segments relative to the reference. Comparisons across resolutions were subsequently used to examine changes in these patterns. This assessment describes visual cartographic agreement and does not constitute a quantitative positional accuracy assessment or independent validation of flood extent or soil saturation. The D8 and D∞ network overlays are presented in Figure 4; the SIGSC reference is not displayed in the figure.

Initially, the derived drainage networks were compared. For the study watershed, the D8 and D∞ networks were overlaid at each resolution, and differences were analyzed in terms of channel location, length, and drainage density. In general, both algorithms were found to identify the main drainage channels at similar locations. However, on divergent slopes and hilltops, D∞ captured dispersed flows that D8 tended to omit or concentrate into single channels. This difference is expected because D∞ distributes flow contributions between up to two adjacent cells and may generate broader flow paths on hillslopes.

In this study, D8 produced drainage networks that were visually clearer and more hierarchical. Clarity, hierarchy, and linearity favor D8 by construction, because D8 routes all flow to a single neighbor. They are not independent evidence of better performance. This routing produces discrete connectivity and linear drainage paths. In this watershed, this facilitated threshold definition and the generation of continuous main drainage axes.

In contrast, D∞ represents flow direction as a continuous angle defined by the local gradient and partitions flow between two downslope cells [6]. It tended to generate more diffuse contribution patterns on smooth surfaces and appeared more sensitive to microvariations in higher-resolution DTMs. This may reduce the stability of channel extraction, because the contributing area becomes distributed and the network may lose cartographic sharpness. This visual impression is not reflected in drainage density: D∞ was less dense than D8 at 1 m (1.51 versus 1.99 km/km$^2$) and nearly equal at 5 m (1.37 versus 1.38 km/km$^2$), although thresholds differed among configurations (Table 1).

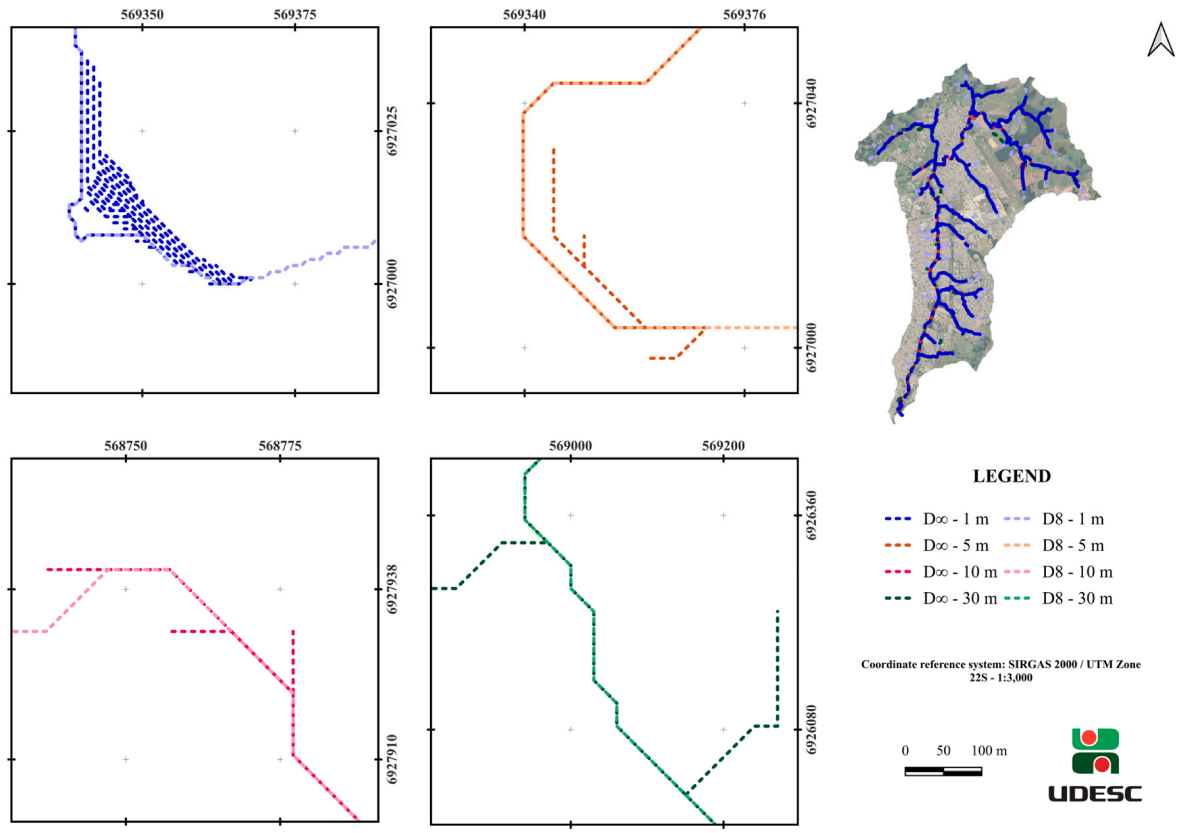


**Figure 4.** Drainage networks generated from the D8 and D∞ algorithms.

These differences should not be read as evidence of the practical superiority of D8. In the current design, algorithm, resolution, and threshold are confounded. Table 1 shows that each configuration was evaluated with its own threshold range. Differences between D8 and D∞ therefore cannot be attributed to the algorithm alone. A factorial design would isolate these effects. It would cross both algorithms with the four resolutions under a common set of equivalent contributing-area thresholds. Each combination would then be evaluated with measurable metrics, such as buffer-based agreement with SIGSC and drainage density. This design would allow the main effects and their interactions to be estimated. It was not implemented here and is recorded as a limitation and future work (Section 3.5). In addition, thresholds were tuned against the same SIGSC reference used to judge agreement (Section 2.2.5). A reference network less detailed than the high-resolution DTMs would tend to favor networks from coarser DTMs. This may bias the agreement criterion toward the coarser configurations.

### *3.2. Effects of DTM Resolution on Drainage Extraction*

The DTMs with 1 m and 5 m spatial resolution capture microdepressions, shallow rills, anthropogenic depressions, ditches, and ephemeral features. When a flow algorithm is applied and a low threshold is adopted, the system tends to interpret these microforms as first-order channels, producing a very dense network that is often disconnected from the structural drainage system. In practice, the product begins to represent a set of microtopographic convergence lines, i.e., flow paths that follow small-scale terrain irregularities, rather than a functional fluvial network. This type of instability is consistent with evidence showing that terrain-derived indices and automated methods are strongly dependent on DTM resolution and preprocessing. Therefore, small changes in the terrain surface alter the convergence pattern and, consequently, the final drainage layout and its associated products [5,27].

When the threshold is increased in these DTMs, the opposite effect occurs. As the algorithm begins to require larger contributing areas to identify a channel, the network collapses into only a few main axes or becomes underrepresented. In process terms, a large-scale rule is imposed on a terrain surface that contains microtopographic signals, resulting in a scale-compatibility problem. This is consistent with findings that the results of hydromorphological-index-based mapping vary with DTM and parameterization choices, affecting product stability [27]. Over-densification at 1 m and 5 m thus results from the interaction between resolution and the chosen threshold. D8 at 1 m used 90,000–110,000 cells ($\approx$0.1 km$^2$). D8 at 30 m used 100–1000 cells ($\approx$0.09–0.9 km$^2$). Hence, the physical contributing areas overlap only near the lower bound.

At 10 and 30 m, the smoothing introduced by mean aggregation acts as a spatial filter that reduces microscale noise. Flow convergence then appears to follow structural thalwegs more closely. This is reflected in visually more continuous, hierarchical, and interpretable networks, with lower sensitivity to the selected threshold. In other words, the network represents features at a scale visually compatible with the watershed area (~26.9 km$^2$) and with the intended mapping scale.

The influence of DTM resolution and parameterization on drainage extraction is illustrated by the mean length and drainage density values presented in Table 1. The 10 and 30 m DTMs produced networks that appeared visually more stable across thresholds. The 1 m DTM produced the highest values for both algorithms, reflecting drainage over-densification. These values were 53.41 km and 1.99 km/km$^2$ for D8 and 40.69 km and 1.51 km/km$^2$ for D$\infty$. The differences between D8 and D$\infty$ were small at 5 and 10 m and more pronounced at 1 and 30 m. D8 was denser than D$\infty$ at 1, 5, and 10 m (by 0.48, 0.01, and 0.06 km/km$^2$) and sparser only at 30 m (by 0.44 km/km$^2$). The low density of D8 at 30 m coincides with the largest equivalent contributing-area range tested (0.09–0.90 km$^2$, versus at most 0.40 km$^2$ in the other configurations), so it should not be read as an algorithm effect. At 1 m, the D8–D$\infty$ difference (0.48 km/km$^2$) exceeds the change in density from 5 m to 10 m within each algorithm (0.09 km/km$^2$ for D8 and 0.14 km/km$^2$ for D$\infty$). Density alone therefore does not separate resolution classes independently of the algorithm. Because thresholds differed among configurations, these differences reflect resolution and threshold choices jointly (Section 3.1). They nevertheless show that the extracted network, and the products derived from it, depend strongly on these choices.

Because the D8 and D$\infty$ contributing-area outputs are expressed in different native units (number of contributing cells and specific catchment area, respectively), the numerical magnitudes of their raw thresholds cannot be directly compared. Therefore, the thresholds adopted in this study were defined and interpreted within the native units of each algorithm; the equivalent contributing areas listed in Table 1 are provided for reference only. The sensitivity analysis showed that the threshold ranges associated with coherent drainage networks varied according to both the flow-direction algorithm and DTM resolution. Comparable network indicators were also obtained with D8 and D$\infty$ under different raw threshold ranges (Table 1). Thus, the observed differences should not be attributed solely to flow partitioning in D$\infty$, but rather to the combined effects of routing formulation, terrain resolution, topographic representation, and threshold parameterization.

This result is consistent with applied studies that have produced flood-related products from intermediate-resolution data. For example, a flood susceptibility study in Candelária, Rio Grande do Sul, Brazil, structured susceptibility classes consistent with local conditions from 30 m SRTM data combined with topographic variables and distance-to-drainage information [28]. That study addressed susceptibility mapping rather than the evaluation of HAND across resolutions or flow-routing algorithms. Our results are therefore consistent with, but not directly equivalent to, its findings, as both suggest that generalized terrain

can support a more stable definition of the drainage system at the watershed scale. That study used native 30 m SRTM data, whereas our 30 m DTM is a mean aggregation of the 1 m DTM. Their error structures differ, which limits direct comparison.

### *3.3. Effects of DTM Resolution on HAND and TWI*

HAND expresses, for each pixel, the relative height above the hydrologically connected channel, that is, the elevation difference to the nearest channel along the terrain connectivity. Thus, HAND behavior is strongly controlled by DTM quality, the coherence of the extracted drainage network, and the connectivity imposed by the flow algorithm [24,25].

With the over-dense networks extracted from the 1 m and 5 m DTMs, nearly every pixel is vertically close to some channel, even an ephemeral one. The result is a HAND distribution concentrated in low values and, consequently, spatially extensive low-HAND patches, because the model measures proximity to microchannels rather than to the main fluvial system. This behavior is consistent with reports that topographic indices may generate false positives when the topography contains excessive microvariability and the drainage network used as input does not represent the functional channel system [25,27].

Purwanto et al. [27], comparing HAND- and TWI-based flood-prone mapping models in data-scarce areas, reported that the performance of these indices depends on how terrain and drainage are represented, with DTM resolution and parameterization affecting the spatial coherence of the final map. Although that study did not evaluate flow-routing algorithms, its findings are consistent with the interpretation that HAND results are more interpretable when the underlying drainage network is hydrologically coherent.

At 10 and 30 m, the extracted network tends to represent the main axes and structural tributaries. HAND then shows progressive altimetric gradients from valley bottoms to lower slopes and interfluves, with low values along thalwegs. This is consistent with environmental applications of HAND that differentiate hydrogeomorphological compartments and patterns of channel proximity at the watershed scale [5]. In the present watershed, these resolutions provided visually more coherent patterns at the scale analyzed. Figure 5 presents the variation observed during the sensitivity analysis for the HAND model.

The HAND and TWI maps in this section were derived only from D8. D8 was selected because it produced visually clearer networks in the drainage-extraction comparison (Section 3.1); this criterion favors D8 by construction. D∞-based HAND and TWI products were not compared with the D8-based products. The patterns described here therefore characterize the effect of DTM resolution under D8 routing only. They do not constitute evidence of the suitability of D8 relative to D∞ for HAND or TWI mapping. Moreover, each resolution used its own network, so DTM and network effects on HAND are confounded. Computing HAND with a common network at all resolutions would separate these effects. This was not done and is recorded as future work.

It should be emphasized that the drainage-extraction threshold must be interpreted according to the native units of each contributing-area product. For D8, the threshold is expressed as the accumulated number of contributing cells, whereas for D∞ it corresponds to TauDEM specific catchment area, expressed in meters (contributing area divided by cell size). Consequently, raw numerical thresholds cannot be directly compared across algorithms or DTM resolutions. For this reason, Table 1 reports the threshold ranges in the native units of each algorithm (number of contributing cells for D8 and specific catchment area for D∞), together with the resulting mean total drainage length and drainage density; the equivalent contributing areas ($km^2$) are listed for reference only. As shown in Table 1, similar drainage densities were obtained from markedly different raw threshold ranges (e.g., 1.29 $km/km^2$ for D8 at 10 m with a threshold range of 1500–2500 and 1.23 $km/km^2$ for D∞ at 10 m with a threshold range of 10,000–30,000), whereas the same raw range (3000–9000)

yielded 1.38 km/km$^2$ for D8 at 5 m and 1.20 km/km$^2$ for D$\infty$ at 30 m. This indicates that raw threshold values cannot be directly compared across different grid resolutions and flow-routing algorithms to explain the resulting drainage network density.

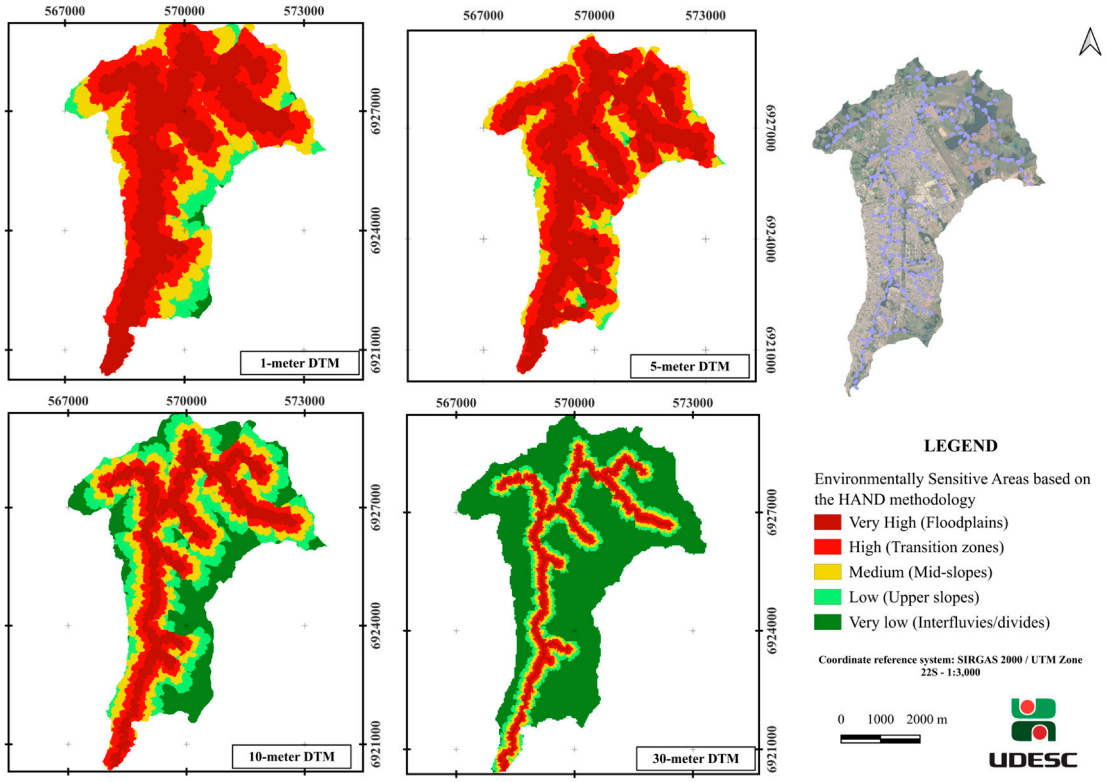


**Figure 5.** HAND-derived environmental sensitivity patterns at DTM resolutions of 1, 5, 10, and 30 m using D8. Colors represent the five HAND-based sensitivity classes, from very high (dark red; floodplains) to very low (dark green; interfluves/divides), as defined in Section 2.2.6.

Therefore, the differences observed in drainage-network extraction are interpreted as the combined effect of DTM resolution, terrain representation, flow-routing formulation, and threshold parameterization, rather than as a direct consequence of cell count. As a general property of threshold-based extraction, a threshold that exceeds the maximum value of the corresponding contributing-area raster leaves no cells satisfying the drainage-initiation criterion and, therefore, produces no drainage network; the upper limits of the ranges in Table 1 remain below this condition for each configuration.

Complementary to HAND, the Topographic Wetness Index (TWI), calculated from the ratio between the specific contributing area and the tangent of the slope, showed behavior that was also sensitive to DTM resolution and to the representation of flow convergence. As with HAND, the application of TWI to high-resolution DTMs (1 m and 5 m) resulted in spatial patterns strongly influenced by topographic microvariability, with amplification of areas classified as having high wetness potential in small concavities, shallow rills, and anthropogenic terrain features. In these cases, the index begins to respond more to local terrain roughness than to the dominant hydrological controls of the watershed, generating fragmented patches that are difficult to interpret at the watershed scale. Figure 6 presents the variation in high-TWI areas, i.e., areas of higher topographic accumulation potential, at each resolution.

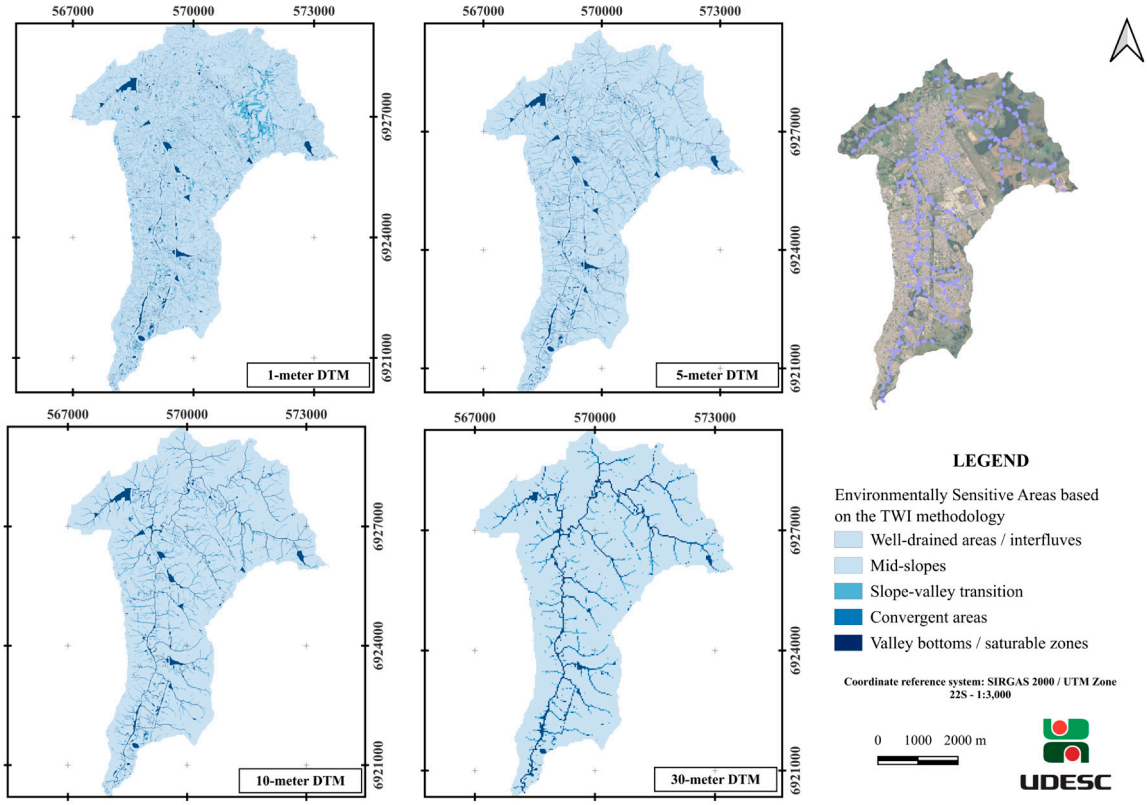


**Figure 6.** TWI-derived environmental sensitivity patterns at DTM resolutions of 1, 5, 10, and 30 m using D8. Blue shades represent the five TWI classes, from well-drained areas/interfluves (lightest) to valley bottoms/saturable zones (darkest).

Index intervals representing different levels of topographic accumulation potential were considered. Higher values indicate greater flow accumulation, typically in valley bottoms; intermediate values correspond to transition zones and convergent slopes; and low values represent well-drained areas in higher topographic positions. Thus, the classification made it possible to distinguish hydrological landscape units with different levels of environmental sensitivity.

In highly detailed DTMs, small altimetric variations produce low local slopes and locally increase contributing areas at the microscale, which inflates TWI values. Consequently, the index tends to assign high values to small concavities and anthropogenic features, which likely overrepresent areas of high accumulation potential, especially in urban and peri-urban environments, where cuts, fills, roads, and surface drainage structures modify the natural morphology. This limitation is widely discussed in the literature, which emphasizes that TWI may produce false positives when applied to surfaces with high topographic heterogeneity or when the DTM scale is not compatible with the analyzed water redistribution processes [10,26,27].

In contrast, the 10 and 30 m DTMs produced more continuous and visually coherent TWI patterns. High values concentrated in valley bottoms, convergent areas, and zones adjacent to the main thalwegs. Slopes and interfluves remained associated with lower index values. This suggests that aggregation at these resolutions reduces the influence of microforms and topographic noise. TWI patterns then more closely reflect the expected topographic control on moisture redistribution, although this was not verified with soil moisture data. These results are consistent with classical applications of TWI, in which the index is used to identify potential patterns of saturation, water accumulation, and surface hydrological connectivity [25,26]. These D8-based patterns do not show that D8 is

preferable for TWI. D∞ and MFD routing were proposed to represent hillslope dispersion better [6,7].

When analyzed together, HAND and TWI showed visually convergent spatial patterns in the 10 and 30 m DTMs. These patterns delineate distinct topographic compartments; their correspondence with flooding or saturation was not verified. In the 1 m and 5 m DTMs, both indices lost interpretability, although through different mechanisms. HAND was mainly affected by the over-densification of the drainage network used as input, whereas TWI was highly sensitive to microscale variations in slope and contributing area. Therefore, for the study watershed and the DTM used, the combined HAND and TWI maps were visually more interpretable at 10 and 30 m, under D8 routing and the thresholds adopted. At these resolutions, the terrain scale appears compatible with the environmental mapping objectives.

### *3.4. Physical and Environmental Relationships*

When interpreted in light of the physical and environmental characterization of the study watershed (Section 2.1), the results suggest that the limitations observed in the application of the HAND model do not arise solely from isolated methodological choices. They may also reflect the interaction between DTM scale and the climatic, pedological, and land use conditions of the watershed. Because these conditions were characterized contextually and were not quantified in the analysis, this relationship is interpretative rather than demonstrated.

The watershed lies in a humid subtropical climate, with no defined dry season, high annual precipitation, and recurrent intense events associated with frontal systems, conditions that can favor rapid hydrological responses and high surface runoff connectivity. This response is likely enhanced by the predominance of clayey Haplic Cambisols, which are associated with low infiltration rates and reduced water storage capacity, and by shallow soils on slopes, which may generate surface runoff by both infiltration excess and saturation excess. In addition, a significant proportion of the watershed is occupied by urban areas and pastures. These land uses tend to increase imperviousness and surface compaction and to reorganize runoff artificially, which can intensify water convergence along roads, embankments, and anthropogenic cuts.

In this setting, the 1 m and 5 m DTMs, with the thresholds adopted, produced visually fragmented HAND patterns at the watershed scale. Their ability to capture topographic microvariations and anthropogenic features resulted in over-densification of the drainage network when combined with threshold-based channel initiation. Ephemeral channels, microvalleys, and surface concentration lines were then treated as structural drainage, so that almost the entire watershed became hydrologically close to some channel. Consequently, HAND showed low values over extensive areas. Visually, these low-HAND zones extended beyond the valley bottoms and reduced the differentiation among landscape compartments.

In contrast, the 10 and 30 m DTMs produced visually more continuous drainage networks and HAND patterns. Aggregation generalizes the terrain and suppresses microtopographic convergence. At these resolutions, the smoothing introduced by aggregation reduces the influence of microfeatures and artificial land use elements, so that the extracted drainage network predominantly follows the main thalwegs. Combined with the thresholds adopted, these DTMs produced visually stable and hierarchical networks. The resulting HAND maps showed progressive gradients of height above drainage, with low values concentrated in valley bottoms and convergent zones. The correspondence of these patterns with fluvial dynamics conditioned by the humid climate and low-infiltration soils is an interpretation of the authors and was not tested against observed flood extents. At 30 m, roads, embankments, culverts, narrow floodplains, and channelized reaches practically disappear

from the terrain surface. These features matter in the urban third of the watershed. The analysis was not stratified between urban and rural areas, so this effect was not quantified.

Two interpretations of these results should be distinguished. First, the results do not demonstrate that coarser resolutions are universally better for HAND or TWI mapping. Second, they indicate that threshold-based channel initiation can be limited when applied to high-resolution microtopography, because a single contributing-area threshold could not simultaneously suppress microtopographic convergence lines and preserve the structural tributaries (Section 3.2). Within this framework, the 10 and 30 m DTMs gave the more interpretable outputs among the tuned configurations. This judgment applies among the configurations evaluated and is based on visual agreement with the SIGSC reference. It reflects their compatibility with the scale of the relevant drainage network, not limitations of the HAND model itself. The 1 m DTM is more detailed altimetrically. However, with threshold-based channel initiation and no additional filtering, it produced less interpretable maps at the watershed scale. Whether high-resolution DTMs would perform comparably after additional filtering, with alternative channel-initiation criteria, or with other preprocessing was not tested in this study. A fair test would hold constant the physical contributing area, a target drainage density, or a common drainage network across resolutions. This was not done and is recorded as a limitation and future work.

### *3.5. Methodological Implications and Limitations*

The two algorithms serve different purposes. In this watershed, D8 produced single-path, continuous channels, which were used as the input network for the HAND maps evaluated. D∞, by distributing flow between adjacent downslope cells, may be more appropriate for representing the dispersion of flow contributions on hillslopes, particularly in divergent or convex terrain. The results therefore do not support a conclusion of universal superiority of either algorithm; rather, they indicate that the choice of algorithm should be consistent with the product of interest.

These methodological implications are restricted to the conditions examined: a single 26.9 $km^2$ watershed, a single DTM derived from a 2012 aerial survey, and coarser resolutions derived from it by aggregation, processed with TauDEM in ArcGIS 10.5. Different behavior may occur with other DTM sources, preprocessing procedures, watersheds, or channel-initiation methods, and the findings should not be extrapolated to such conditions without further testing. The 30 m DTM is a mean aggregation of the 1 m DTM, not a native product such as SRTM or ALOS. Native products carry their own acquisition and surface-object errors. This limits comparison with studies based on native coarse DTMs, such as [28].

The observed results of this study comprise the drainage lengths and densities in Table 1 and the spatial patterns of the drainage networks and of the HAND and TWI maps (Figures 4–6). The association of these patterns with floodplains, saturation-prone areas, climate, soils, and land use is an interpretation of the authors. Several aspects require additional validation. First, the positional agreement of the extracted networks with reference hydrography was assessed only visually. Second, the correspondence of HAND and TWI classes with observed flood extents and soil moisture was not evaluated. No records of the 2005, 2008, or 2011 floods were used. Third, D8- and D∞-based HAND and TWI products were not compared. Fourth, the effect of the temporal difference between the 2012 DTM and the land use and land cover data was not assessed. Fifth, algorithm, resolution, and threshold were confounded, because each configuration used its own threshold range (Table 1). A factorial design with common equivalent-area thresholds and measurable agreement metrics is recommended for future work (Section 3.1). Sixth, no repetitions, alternative conditioning methods, or comparisons with MFD were performed; MFD is cited

only as context in the Introduction. Seventh, the analysis was not stratified between urban and rural areas.

## 4. Conclusions

The results indicate that Digital Terrain Model (DTM) resolution, together with threshold choice, influenced the stability and coherence of the hydromorphological products. The study area was the 26.9 $km^2$ partially urbanized Ponte Grande River watershed. The analysis used the 1 m SIGSC DTM from a 2012 aerial survey and the 5, 10, and 30 m versions aggregated from it. The configurations were compared on the basis of geomorphological coherence, threshold stability, and visual agreement with the SIGSC hydrographic reference. Among the configurations evaluated in this watershed, the 10 and 30 m DTMs produced the visually more stable drainage networks under the thresholds adopted, and D8-based HAND and TWI maps with greater cartographic interpretability. With their thresholds, these resolutions avoided the over-densification observed in the high-resolution configurations. Because thresholds were tuned against the same reference, this result may favor coarser DTMs.

The differences between D8 and D∞ were visible mainly in flow dispersion: D∞ produced more diffuse flow patterns, whereas D8 produced more concentrated and hierarchical networks, a criterion that favors D8 by construction. Drainage density was lower for D8 than for D∞ only at 30 m (0.76 and 1.20 km/$km^2$); at 1, 5, and 10 m it was higher or equal (differences of 0.48, 0.01, and 0.06 km/$km^2$). The low density of D8 at 30 m coincides with the largest threshold range tested (equivalent area of up to 0.90 $km^2$, versus at most 0.40 $km^2$ in the other configurations). Satellite imagery supported only the visual presence of channels, not flood or saturation zones. Because each configuration used its own threshold range, these differences cannot be attributed to the algorithm alone.

Thus, the 10 and 30 m DTMs provided the more visually interpretable basis for the D8-based HAND and TWI maps, and the 30 m configuration had the lowest drainage density. This does not imply that D8 is preferable for TWI. This finding holds only for the configurations evaluated in this watershed and is based on visual agreement with the SIGSC reference. It should not be generalized to other watersheds or DTMs. D∞ may remain relevant for representing hillslope flow contributions. Future applications in this watershed could adopt these configurations as a starting point, provided that they are tested with quantitative agreement metrics and observed flood records.

This study has limitations. The drainage networks were compared only visually with the SIGSC hydrographic reference and satellite imagery, without quantitative positional-accuracy metrics. The HAND and TWI patterns were not validated against observed flood extents or soil moisture measurements. Algorithm, resolution, and threshold were also confounded, because thresholds differed among configurations. The HAND and TWI maps were derived only from D8, and the 2012 DTM and the land use and land cover data refer to different periods. In addition, the analysis was restricted to a single watershed and to resampled versions of a single DTM. No repetitions, alternative conditioning methods, or MFD comparisons were performed. Future work should apply a factorial design with common equivalent-area thresholds. It should also compute D∞-based HAND and TWI, and HAND with a common network across resolutions. It should further incorporate quantitative agreement metrics, observed flood records, and additional watersheds to test the transferability of these findings.

**Author Contributions:** Conceptualization, P.H.L.d.R.; methodology, P.H.L.d.R.; formal analysis, P.H.L.d.R.; visualization, P.H.L.d.R.; writing—original draft preparation, P.H.L.d.R.; writing—review and editing, D.P.R., E.A.S.S., L.J.B. and N.A.N.d.S.; supervision, D.P.R., E.A.S.S., L.J.B. and N.A.N.d.S. All authors have read and agreed to the published version of the manuscript.

**Funding:** This research did not receive any specific grant from funding agencies in the public, commercial, or non-profit sectors.

**Data Availability Statement:** The 1 m digital terrain model and the hydrographic database used in this study were obtained from the Geographic Information System of Santa Catarina (SIGSC). Land use and land cover data were obtained from the MapBiomas Project (Collection 8) [12]. These third-party data are subject to the access conditions of their providers. The datasets, geoprocessing routines, and scripts generated during the current study are not publicly available because they are part of an ongoing research project. They are available from the corresponding author upon reasonable request, subject to institutional and project-related restrictions. The software, tools, processing steps, and threshold ranges used are described in Section 2 and Table 1.

**Acknowledgments:** The authors gratefully acknowledge the support provided by the Santa Catarina State University (Universidade do Estado de Santa Catarina, UDESC), the Graduate Program in Environmental Sciences (PPGCAMB), the Center for Agroveterinary Sciences (CAV), and the Laboratory of Technology-Based Solutions (LATEC). The authors also acknowledge the support received through research scholarships and thank the Santa Catarina Research and Innovation Foundation (FAPESC), the National Council for Scientific and Technological Development (CNPq), and UDESC, as applicable. The authors are thankful for the encouragement, technical support, and institutional infrastructure provided by these institutions and research units, which contributed to the successful development of this study. During the preparation of this manuscript, the authors used Claude (Anthropic; version sonnet 5.5) to support the improvement of the English translation and linguistic fluency of the manuscript, and Gemini Pro 3 (Google; banana pro) to assist in refining Figure 3. These tools were used exclusively for linguistic improvement and figure refinement, respectively, without altering the scientific content, interpretation, methodology, or conclusions. The authors reviewed and edited all outputs and take full responsibility for the content of this publication.

**Conflicts of Interest:** The authors declare no conflicts of interest.

## References

1. Ferreira, G.F.; Veról, A.P.; Mattos, R.R. Design strategies for flood mitigation: A case study in Realengo, Rio de Janeiro. *Rev. Cient. ANAP Bras.* **2023**, *16*, 63–78. [CrossRef]
2. Apaza, G.S.Q.; Ventura, K.S.; Menezes, D.B. Environmental risk analysis in the Monjolinho River, São Carlos, São Paulo. *Periód. Téc. Cient. Cid. Verdes* **2024**, *12*, 197–212. (In Portuguese) [CrossRef]
3. Naves, F.E.; Almeida, R.T.S. Topographic Wetness Index as a method for identifying flooding points in urban areas. *Soc. Territ.* **2021**, *33*, 209–227. [CrossRef]
4. Guasselli, L.A.; Simioni, J.P.D.; Laurent, F. Mapping and classification of wetlands using the Topographic Wetness Index (TWI) from Digital Elevation Models in the Gravataí River watershed, Rio Grande do Sul, Brazil. *Rev. Bras. Geomorfol.* **2020**, *21*, 639–659. [CrossRef]
5. Neto, S.L.R.; dos Santos, V.J.; Schutz, E.L.D.; de Moliner, L.M.; Kloth, C.G.; Schier, D.T.; Othman, A.A.; Liesenberg, V.; Bispo, P.d.C. Application of hydro-based morphological models for environmental assessment of watersheds. *ISPRS Int. J. Geo-Inf.* **2023**, *12*, 314. [CrossRef]
6. Tarboton, D.G. A new method for the determination of flow directions and upslope areas in grid digital elevation models. *Water Resour. Res.* **1997**, *33*, 309–319. [CrossRef]
7. Quinn, P.; Beven, K.; Chevallier, P.; Planchon, O. The prediction of hillslope flow paths for distributed hydrological modelling using digital terrain models. *Hydrol. Process.* **1991**, *5*, 59–79. [CrossRef]
8. Wolock, D.M.; McCabe, G.J. Comparison of single and multiple flow direction algorithms for computing topographic parameters in TOPMODEL. *Water Resour. Res.* **1995**, *31*, 1315–1324. [CrossRef]
9. Silveira, R.M.P.; Silveira, C.T. Geomorphometric method for mapping hilltops, ridges, and valleys. *Rev. Bras. Geomorfol.* **2020**, *21*, 697–717. [CrossRef]
10. Sørensen, R.; Seibert, J. Effects of DEM resolution on the calculation of topographical indices: TWI and its components. *J. Hydrol.* **2007**, *347*, 79–89. [CrossRef]
11. Universidade do Estado de Santa Catarina (UDESC). *Meta 1—Studies and Concepts: Report on Hydrological Concepts*; Technical Report, Contract No. 09/2019, Meta 1, Product 2; Center for Agroveterinary Sciences, Hydrology Laboratory: Lages, Brazil, 2019; Unpublished.

12. MapBiomas Project. Collection 8 of the Annual Land Use and Land Cover Maps of Brazil, 1985–2022. 2023. Available online: https://brasil.mapbiomas.org/faq/ (accessed on 30 September 2026).
13. Instituto Brasileiro de Geografia e Estatística (IBGE). *Biomas e Sistema Costeiro-Marinho do Brasil: Compatível com a Escala 1:250 000*; Relatórios Metodológicos; IBGE: Rio de Janeiro, Brazil, 2019; Volume 45, 168p, ISBN 978-85-240-4510-3. Available online: https://biblioteca.ibge.gov.br/visualizacao/livros/liv101676.pdf (accessed on 30 September 2026).
14. Alvares, C.A.; Stape, J.L.; Sentelhas, P.C.; Gonçalves, J.L.M.; Sparovek, G. Köppen's climate classification map for Brazil. *Meteorol. Z.* **2013**, *22*, 711–728. [CrossRef] [PubMed]
15. Pandolfo, C.; Braga, H.J.; Silva Júnior, V.P.; Massignan, A.M.; Pereira, E.S.; Thomé, V.M.R.; Valci, F.V. *Atlas Climatológico do Estado de Santa Catarina*; Epagri: Florianópolis, Brazil, 2002; CD-ROM. Available online: https://ciram.epagri.sc.gov.br/index.php/solucoes/climatologia/ (accessed on 30 September 2026).
16. Instituto Nacional de Meteorologia (INMET). *Normais Climatológicas do Brasil 1991–2020*; INMET: Brasília, Brazil, 2022. Available online: https://portal.inmet.gov.br/normais (accessed on 30 September 2026).
17. Horton, R.E. The role of infiltration in the hydrologic cycle. *Trans. Am. Geophys. Union* **1933**, *14*, 446–460. [CrossRef]
18. Perrin, J.L.; Bouvier, C.; Janeau, J.L.; Ménez, G.; Cruz, F. Rainfall/runoff processes in a small peri-urban catchment in the Andes mountains: The Rumihurcu Quebrada, Quito (Ecuador). *Hydrol. Process.* **2001**, *15*, 843–854. [CrossRef]
19. Costa, A.; Albuquerque, J.A.; Costa, A.; Pértile, P.; Silva, F.R. Water retention and availability in soils of the State of Santa Catarina, Brazil: Effect of textural classes, soil classes and lithology. *Rev. Bras. Ciênc. Solo* **2013**, *37*, 1535–1548. [CrossRef]
20. Dunne, T.; Black, R.D. Partial area contributions to storm runoff in a small New England watershed. *Water Resour. Res.* **1970**, *6*, 1296–1311. [CrossRef]
21. Zhang, G.; Cui, P.; Gualtieri, C.; Zhang, J.; Ahmed Bazai, N.; Zhang, Z.; Wang, J.; Tang, J.; Chen, R.; Lei, M. Stormflow generation in a humid forest watershed controlled by antecedent wetness and rainfall amounts. *J. Hydrol.* **2021**, *603*, 127107. [CrossRef]
22. Santa Catarina State Government. *Raster Data Metadata of the Aerophotogrammetric Survey of the State of Santa Catarina (2010–2012)*; SIGSC: Florianópolis, Brazil, 2016. Available online: https://sigsc.sc.gov.br/documentacao.html (accessed on 13 October 2026). (In Portuguese)
23. O'Callaghan, J.F.; Mark, D.M. The extraction of drainage networks from digital elevation data. *Comput. Vis. Graph. Image Process.* **1984**, *28*, 323–344. [CrossRef]
24. Rennó, C.D.; Nobre, A.D.; Cuartas, L.A.; Soares, J.V.; Hodnett, M.G.; Tomasella, J.; Waterloo, M.J. HAND, a new terrain descriptor using SRTM-DEM: Mapping terra-firme rainforest environments in Amazonia. *Remote Sens. Environ.* **2008**, *112*, 3469–3481. [CrossRef]
25. Nobre, A.D.; Cuartas, L.A.; Hodnett, M.; Rennó, C.D.; Rodrigues, G.; Silveira, A.; Waterloo, M.; Saleska, S. Height Above the Nearest Drainage: A hydrologically relevant new terrain model. *J. Hydrol.* **2011**, *404*, 13–29. [CrossRef]
26. Beven, K.J.; Kirkby, M.J. A physically based variable contributing area model of basin hydrology. *Hydrol. Sci. Bull.* **1979**, *24*, 43–69. [CrossRef]
27. Purwanto, A.; Andrasmoro, D.; Eviliyanto, E. Comparative analysis of HAND with TWI flood-prone mapping models in data-scarce areas. *Indones. J. Geogr.* **2025**, *57*, 227–235. [CrossRef]
28. Silva, W.O.; Robaina, L.E.S.; Tretin, R.; Sccoti, A.A.V. Automated relief study: A proposal for defining areas susceptible to flooding in Candelária, Rio Grande do Sul. *Rev. Geogr.* **2024**, *41*, 75–92. [CrossRef]


**Disclaimer/Publisher's Note:** The statements, opinions and data contained in all publications are solely those of the individual author(s) and contributor(s) and not of MDPI and/or the editor(s). MDPI and/or the editor(s) disclaim responsibility for any injury to people or property resulting from any ideas, methods, instructions or products referred to in the content.